Theoretical Raman and FTIR vibrational analysis of 2-phenyl-1H-indene-1,3(2H)-dione by *ab initio* method

Jitendra Pathak, Vijay Narayan, Leena Sinha*, and Onkar Prasad

Physics Department, University of Lucknow, Lucknow, Pin Code - 226007, India

Abstract. 2-phenyl-1H-indene-1,3(2H)-dione is an anticoagulant and functions as a Vitamin K antagonist. The equilibrium geometries and harmonic frequencies of the molecule under investigation was determined and analyzed at DFT level employing the basis set 6-311++G(d,p). The skeleton of the optimized molecules is found to be non-planar. The plane of the phenyl ring and the mid-plane of the bicyclic moiety are almost perpendicular to each other. In general, a good agreement between experimental and calculated normal modes has been observed. A comparison of calculated frontier orbital energy gap 2-phenyl-1H-indene-1,3(2H)-dione and 1H-indene-1,3(2H)-dione shows that the 2-phenyl-1H-indene-1,3(2H)-dione is slightly more reactive molecule than its parent. The other molecular properties of 2-phenyl-1H-indene-1,3(2H)-dione like dipole moment, polarizability, MESP potential surface have also been calculated and compared with the parent molecule.

PACS: 31.15.E-, 31.15.ap, 33.20.Tp

Key words: anticoagulant, geometry optimization, molecular electrostatic potential surface, normal mode analysis

1 Introduction

In conjunction with heparin, the use of oral anticoagulant drug therapy has become a focus of immense academic and pharmaceutical interest. Anticoagulant therapy is a course of drug therapy in which anticoagulant medications are administered to a patient to inhibit the formation of clotting agents so that the blood cannot clot easily. The drug 2-phenyl-1H-indene-1,3(2H)-dione also known as phenindione, an indandione (1H-indene-1,3(2H)-dione) derivative, has been used as an anticoagulant and functions as vitamin K antagonist. Phenindione which is a 1,3-diketone carbon acid, thins the blood and is used when the patient is allergic to warfarin [1, 2]. Pipkin, and Stella have carried out the study of tautomerism of

---

*Corresponding author. *Email address:* sinhaleena27@gmail.com (L. Sinha)

phenindione, 2-phenyl-1,3-indandione, in dipolar aprotic/hydrocarbon solvent mixtures and have reported that phenindione exists predominantly in its diketo, rather than enol form in hydrocarbon solvents [3].

The aim of present communication is to investigate the molecular structural, vibrational and energetic data analysis of the molecule under study, in gas phase, due to its biological and pharmaceutical importance. The structure and ground state energy of the molecule under investigation has been analyzed by employing DFT/B3LYP level. In order to obtain more complete description of molecular motion, vibrational frequency calculation has been carried out at the DFT level. The reported geometries, molecular properties such as equilibrium energy, dipole moment, polarizability and vibrational frequencies along with electrostatic potential maps, have also been used to understand the properties of the title molecule.

2   Experimental

The model molecular structure of phenindione along with its parent molecule has been given in Fig. 1. The calculated vibrational spectra plotted in Figs. 2 and 3, has been matched with FT-IR and FT-RAMAN spectra obtained from Sigma Aldrich website [4].
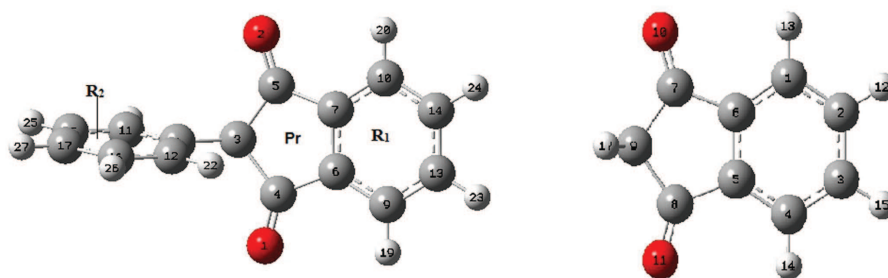
Figure 1: Optimized structure of 2-phenyl-1H-indene-1,3(2H)-dione and 1H-indene-1,3(2H)-dione.

3   Computational details

The Becke's three parameter hybrid exchange functional [5] with Lee-Yang-Parr correlation functionals (B3LYP) [6,7] of the density functional theory [8] and 6-311++G (d,p) basis set were chosen to optimize the structures of the molecules under investigation. All the calculations were performed using the Gaussian 09 program [9]. Positive values of all the calculated vibrational wave numbers confirmed the geometry to be located at true local minima on the potential energy surface. As the DFT hybrid B3LYP functional tends to overestimate the fundamental normal modes of vibrations, a uniform scaling factor of 0.9679 [10,11] has been applied and in general a good agreement of calculated modes with experimental ones has
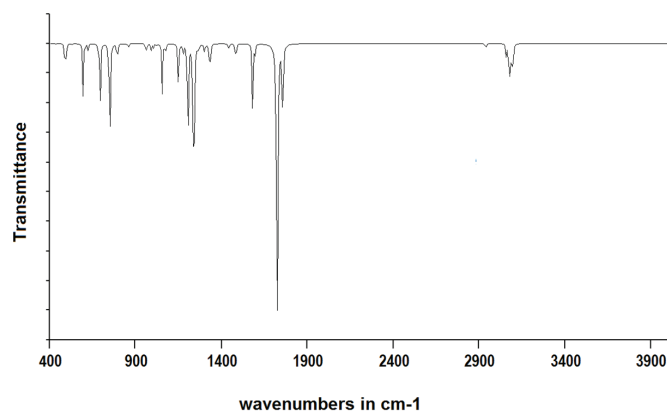
Figure 2: Theoretical IR spectra of 2-phenyl-1H-indene-1,3(2H)-dione.
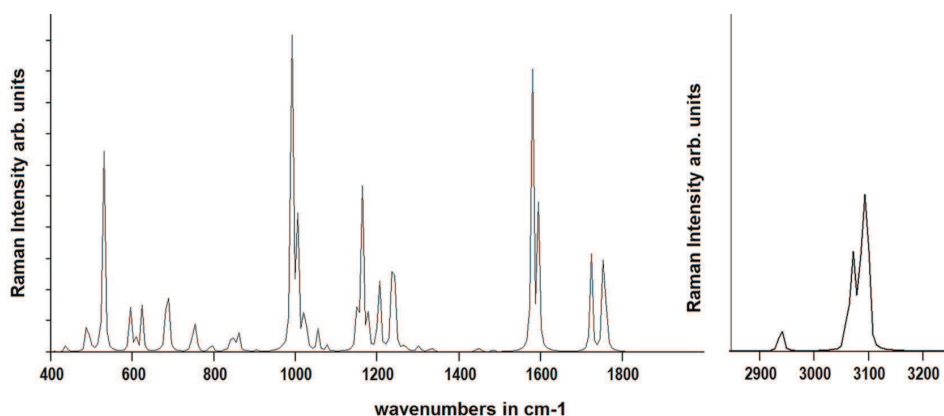
Figure 3: Theoretical Raman spectra of 2-phenyl-1H-indene-1,3(2H)-dione.

been obtained. The vibrational wavenumber assignments have been carried out by combining the results of the Gaussview 5.08 program [12], symmetry considerations and the VEDA 4 program [13]. The absolute Raman intensities were calculated from the Raman activities (S_i), obtained with the Gaussian 09 program, and using the following relationship derived from the intensity theory of Raman scattering [14, 15]

$$I_i = \frac{f(v_0 - v_i)^4 S_i}{v_i \exp\left(\frac{-hcv_i}{kT}\right)},$$

where v_0 being the exciting wave number in cm^{-1}, vi the vibrational wave number of i-th normal mode, h, c and k universal constants and f is a suitably chosen common normalization factor for all peak intensities. The calculated Raman and IR spectra have been plotted using the pure Lorentzian band shape with a band width of FWHM of 5 cm^{-1} and are shown

in Figs. 2 and 3. The density functional theory has also been used to calculate the dipole moment and mean polarizability $\langle \alpha \rangle$ are given in terms of x, y, z components by the following equations

$$\mu = \left(\mu_x{}^2 + \mu_y{}^2 + \mu_z{}^2 \right)^{\frac{1}{2}},$$
$$\langle \alpha \rangle = \frac{1}{3}(a_{xx} + a_{yy} + a_{zz}).$$

4   Results and discussion

4.1   Geometry optimization

The structure of 1H-indene-1,3(2H)-dione which is the ancestor of the phenindione has also been investigated as a reference, in order to assess the effect of introduction of a phenyl group at the flap carbon position. The equilibrium geometry optimization for both the molecules has been achieved by energy minimization, using DFT at the B3LYP level, employing the basis set 6-311++G(d,p). The optimized geometry of both molecules under study are confirmed to be located at the local true minima on potential energy surface, as the calculated vibrational spectra has no imaginary frequency. The X-ray diffraction data of the phenindione and 1H-indene-1,3(2H)-dione, obtained from Dug Bank [16] and Cambridge Crystallographic Data Centre (CCDC) respectively, have been used to optimize the structures. The optimized molecular structures thus obtained representing the numbering scheme of the atoms are shown in Fig. 1. The optimized geometrical parameters of both the molecules have been compared with the previous X-ray study of 1H-indene-1,3(2H)-dione reported by Chetkina and Belsky [17], which further confirm the optimization of both the molecules under investigation. Like its parent, this compound exists in two forms in organic solvents owing to the keto-enol tautomerism and only in the diketone form in the crystal.

    In case of 2-phenyl-1H-indene-1,3(2H)-dione and its parent molecule, the five-membered ring adopts an envelope conformation, with the C(3)/C(9) atoms, acting as the flap atom, deviating from the plane through the remaining four carbon atoms. In case of 2-phenyl-1H-indene-1,3(2H)-dione/ 1H-indene-1,3(2H)-dione, the values of the bond lengths of five membered ring are in the range 1.55 Å–1.40 Å and the C(4)=O(1)/C(7)=O(10) and C(5)=O(2)/C(8)=O(11) bond length both equal to 1.21 Å are also found to be close to the standard C=O bond length (1.22 Å) [23, 24]. The benzene endocyclic C-C-C angles in 2-phenyl-1H-indene-1,3(2H)-dione/1H-indene- 1,3(2H)-dione are found to decrease to 117.8°/117.9° at C(9)/C(1) and C(10)/C(4) atoms and increased on an average to 121.1°/121.4° at other remaining carbon atoms. For the five-membered ring in both cases, the endocyclic angles are equal to 103.9°/105.1° at C(3)/C(9), 107.7°/107.2° (on an average) at C(5)/C(8) and C(4)/C(7), and 110.4°/109.2° at the C(6)/C(6) and C(7)/C(5) atoms. These DFT calculated bond length, bond angles are in full agreement with those reported in Chetkina and Belsky [17]. The skeleton of both the molecules is not strictly planar. The dihedral angles C(5)–C(6)–C(7)–C(9) and C(6)–C(5)–C(8)–C(9) which represent the angular separa-

tion/orientation of flap atom C(9) with respect to plane of the molecule, are found to be 0.02° and -0.02° for 1H-in-dene-1,3(2H)-dione, respectively. But in case of Phenindione, the corresponding dihedrals containing the flap atom C(3) assumes a higher value 1.8° and -1.4°. It is seen that most of the bond distances are similar in both the molecules although there are differences in molecular formula. In the six-membered rings all the C–C bond distances are 1.39-1.40 Å, while in the five-membered rings the C-C bond distances vary from 1.20 Å to 1.54 Å. The C-H bond lengths remained between 1.08 Å and 1.10 Å in both the molecules considered [18].

4.2   Electronic properties

The most important orbitals in a molecules are the frontier molecular orbitals, called highest occupied molecular orbital (HOMO) and lowest unoccupied molecular orbital (LUMO). These orbitals determine the way the molecule interacts with other species. The frontier orbital gap helps characterize the chemical reactivity and kinetic stability of the molecule. A molecule with a small frontier orbital gap is more polarizable and is generally associated with a high chemical reactivity, low kinetic stability and is also termed as soft molecule [19]. The lower value for frontier orbital gap in case of 2-phenyl-1H-indene-1,3(2H)-dione than 1H-indene-1,3(2H)-dione makes it slightly more reactive and less stable (Table 1). The HOMO is the orbital that primarily acts as an electron donor and the LUMO is the orbital that largely acts as the electron acceptor. The 3D plots of the frontier orbitals HOMO and LUMO and the molecular electrostatic potential map (MEP) figures for both molecules are shown in Figs. 4 and 5. It can be seen from the Fig. 4 that, the HOMO of phenindione is delocalized over the entire molecule except ring R_1 and has more antibonding character than its parent molecule. The LUMO in case of both the molecule looks similar. All the HOMO and LUMO have nodes. The nodes in each HOMO and LUMO are placed symmetrically. The MESP which is a plot of electrostatic potential mapped onto the constant electron density surface is shown in Fig. 5. The molecular electrostatic potential surfaces make clear that even when the two molecules are structurally very similar; this similarity does not carry over into their electrophilic/nucleophilic reactivities. The resulting molecular electrostatic potential surface mapped in terms of colour grading and is very useful tool in investigation of correlation between molecular structure and the physiochemical property relationship of molecules including biomolecules and drugs [20–26]. The variation in electrostatic potential produced by a molecule is largely responsible for the binding of a drug to its receptor binding sites, as the binding site in general is expected to have opposite areas of electrostatic potential.

The MESP map in case of 2-phenyl-1H-indene-1,3(2H)-dione and 1H-indene-1,3(2H)-dione clearly suggests that the potential swings wildly between carbonyl oxygen atoms (dark red) and five-membered ring (blue). The carbonyl oxygen atoms reflect the most electronegative region and have excess negative charge, and the hydrogen atoms attached to the benzene ring bear the brunt of positive charge (blue region). The MESP of phenindione reveals larger electron rich area as compared to its parent molecule. The values of the extreme potentials for MESP maps of both molecules have been taken same for the sake of comparison and drawing
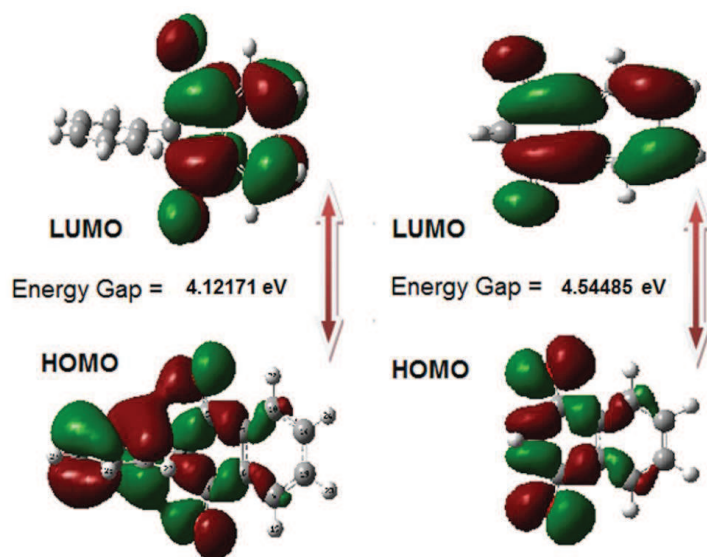
Figure 4: HOMO-LUMO of 2-phenyl-1H-indene-1,3(2H)-dione and 1H-indene-1,3(2H)-dione.
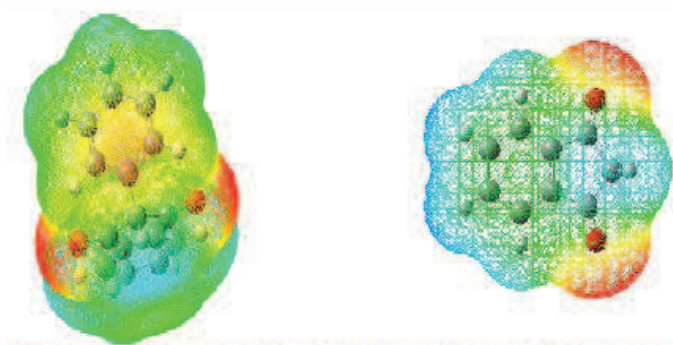
Figure 5: MESP maps of 2-phenyl-1H-indene-1,3(2H)-dione and 1H-indene-1,3(2H)-dione.

Table 1: Theoretically computed ground state optimized parameters.

S. No.	Parameters	B3LYP/6-311++G(d,p)	
		2-phenyl-1H-indene-1,3(2H)-dione	1H-indene-1,3(2H)-dione
1	Ground State Energy (in Hartree)	-728.26016	-497.15701
2	Frontier Orbital energy gap (in Hartree)	0.15147	0.16702
3	Dipole moment (in Debye)	3.0618	3.3104
4	Polarizability (in a.u.)	176.7	107.0

the conclusions. A closer inspection of various plots given in Figs. 4 and 5 and the electronic properties listed in Table 1, one can easily conclude how the substitution of the hydrogen atoms by a phenyl group modifies the properties of the ancestor molecule. The dipole moment in a molecule is another important electronic property that results from non-uniform distribution of charges on the various atoms in a molecule. It is mainly used to study the intermolecular interactions involving the van der Waal type dipole-dipole forces, etc., because larger the dipole moment, stronger will be the intermolecular interactions. It is also clear from the Table 1 that although the values of dipole moment of the two molecules vary within 10%, yet the mean polarizability varies significantly.

4.3 Vibrational analysis

The optimized molecular structure belongs to the C1 point group as it does not display any special symmetry. As a result of this all the normal modes of phenindione are found to be both infrared and Raman active. The overestimate of the wavenumbers by DFT and the anharmonicity corrections are taken care by calibrating vibrational wavenumber with scaling 0.9679 for DFT at B3LYP [10, 11]. The vibrational assignments have been done on the basis of relative intensities, line shape, the VEDA 4 program and the animation option of Gaussview 3.0. The experimental and scaled calculated wavenumbers along with their respective dominant normal modes are presented in Table 2.

Table 2: The calculated and experimrntal* wavenumbers (in cm^{-1}) at B3LYP/6-311++G(d,p) with their relative intensities and probable assignments with potential energy distribution of 2-phenyl-1H-indene-1,3(2H)-dione.

S. No.	Unsc. wave No.	Scaled wave No.	Exp. IR*	Exp. Raman*	IR intensity	Raman intensity	Assignments
1	3198	3096	–	–	12.67	15.74	ν(C–H)R_1(96)
2	3195	3092	3092	3085	2.49	2.06	ν(C–H)R_1(95)
3	3191	3089	3089	3085	15.28	17.78	ν(C–H)R_2(82)
4	3184	3081	–	3085	5.17	7.64	ν(C–H)R_1(96)
5	3180	3078	–	3085	26.42	2.43	ν(C–H)R_2(82)
6	3172	3070	–	3065	8.10	5.62	ν(C–H)R_2(85)
7	3171	3069	–	3065	1.55	3.13	ν(C–H)R_1(95)
8	3163	3061	3042	3056	1.33	3.46	ν(C–H)R_2(82)
9	3157	3055	3042	3045	7.65	1.57	ν(C–H)R_2(80)
10	3034	2936	2935	2920	4.89	4.88	ν(C3–H18)(100)
11	1810	1752	1747	1748	87.18	19.83	νs(C–O)Pr(88)
12	1776	1719	1714	1710	439.49	10.38	νas(C–O)Pr(90)
13	1644	1591	1599	1600	6.24	14.22	ν(C–C)R_2 (50) + β(H–C–C)R_2(40)
14	1629	1576	1585	1590	41.13	23.38	ν(C–C)R_1 (40) + β(H–C–C)R_1(40)
15	1627	1574	1585	1590	1.83	4.08	ν(C–C)R_1 (40) + β(H–C–C)R_1(30)
16	1625	1572	1585	1564	1.50	3.84	ν(C–C)R_2 (40) + β(H–C–C)R_1(30)
17	1527	1478	1480	1470	16.81	0.30	β(H–C–C)+ R_2(50)+ν(C–C)R_2(20) [semi circular str.]
18	1492	1444	1453	–	0.03	0.19	β(H–C–C)R_1(50)+ν(C–C)R_1(25)
19	1491	1444	1453	–	0.14	0.29	β(H–C–C)R_1(50)+ν(C–C)R_1(20)
20	1484	1436	–	–	5.27	0.25	β(H–C–C)R_2(55)+ν(C–C)R_2(20)
21	1371	1327	1326	1350	27.82	0.66	ν(C–C)R_1(65)+β(H–C–C)R_1(15)
22	1364	1320	1304	1327	4.23	0.11	β(H–C–C)R_2(85)+ β(H18–C3–C8)(10)

Table 2: (Continued).

S. No.	Unsc. wave No.	Scaled wave No.	Exp. IR*	Exp. Raman*	IR intensity	Raman intensity	Assignments
23	1340	1297	1289	1290	7.38	0.87	ν(C–C)R_2(57)+β(H–C–C)R_2(12)+β(H18–C3–C8)(17)
24	1304	1262	1261	1278	4.69	0.99	β(H–C–C)R_1(45)+β(C–C–C) R_1 (20)
25	1274	1233	1225	1240	218.25	22.91	β(H–C–C)R_2(45)+ν(C3–C8)(25)+ β(H18–C3–C8)(20)
26	1239	1199	1186	1174	88.87	10.85	β(H18–C3–C8)(22)+β(H–C–C)R_2(20)+β(H–C–C)R_1(18) + ν(C–C)Pr(15)
27	1210	1171	1178	1170	4.74	2.91	wag(C3–H18)(60)+β(H–C–C)R_2(11)+β(H–C–C)R_1(10)
28	1207	1168	1160	1155	0.60	1.55	β(H–C–C)R_2(40)+wag (C3–H18) (17)
29	1195	1157	1150	1155	0.39	17.24	wag (C3–H18) (52) + β(H–C–C)R_2(13)
30	1191	1153	1150	–	0.63	1.38	β(H–C–C)R_1(33)+ wag (C3–H18) (27)
31	1183	1145	–	1146	0.18	1.20	β(H–C–C)R_2(87)
32	1181	1143	1150	–	23.42	2.92	β(H–C–C)R_1(70) + wag (C3–H18) (11)
33	1106	1071	1074	1060	0.06	0.51	β(H–C–C)R_1(49)+β(C–C–C)R_1(25)+wag(C3–H18) (10)
34	1103	1068	1067	–	8.45	0.10	β(H–C–C) R_2(66) +β(H18–C3–C8)(10)
35	1084	1049	1031	1037	33.33	2.17	β(H–C–C)R_1(40)+wag(C3–H18)(20)+ β(H–C–C)R_2(10)
36	1050	1016	1016	–	1.59	7.96	β(H–C–C)R_2(72) + β(C–C–C) R_1 (20)
37	1030	997	1002	1000	4.22	19.43	ν(C–C)R_1(33) + β(H–C–C)R_1(25)+ β(C–C–C)R_1(11)
38	1017	985	–	987	0.01	0.02	wag(C–H)R_1(83)
39	1017	985	979	987	4.04	29.99	Trigonal Bending R_2(74) + wag(C–H)R_1(23)
40	1000	968	–	–	0.07	0.01	wag(C–H)R_2(85)
41	993	961	–	–	1.28	0.20	wag(C–H)R_1(84)
42	985	953	–	–	5.60	0.14	ν(C–C)Pr(38)+wag(C–H) R_1(21)
43	980	949	–	937	0.06	0.02	wag(C–H)R_2(83)
44	926	897	–	–	0.18	0.14	wag(C–H)R_2(78)
45	909	880	868	870	0.06	0.11	wag(C–H)R_1(84)
46	880	852	–	–	3.80	3.40	β_{out}(O–C–C)Pr (44) + wag (C–H) R_1 (21)
47	864	837	819	–	0.27	3.37	wag(C–H)R_1(24)+wag(C–H)R_2(22)+ β_{out}(O–C–C)Pr (16)
48	850	822	819	819	0.04	0.27	wag(C–H)R_2(88)
49	813	786	770	–	15.58	1.40	β(C–C–C) Pr(34)+β(C–C–C) R_1(28)+β(C–C–C)R_2(20)
50	776	751	756	–	0.44	0.72	β_{out}(C–C–C)R_1(36)+ β_{out}(C–C–C)Pr (26)+ β_{out}(O–C–C)Pr (14)
51	771	746	–	–	55.03	2.45	wag(C–H)R_1(44)+ wag(C–H)R_2(12)
52	762	738	729	728	21.29	1.04	wag(C–H)R_2(53)+ β(C4–C3–C8)(26)+ wag(C–H)R_1(18)
53	710	687	–	695	50.11	0.03	wag(C–H) R_2 (60)
54	701	679	–	–	1.90	8.26	β(O–C–C)Pr(26) + wag(C–H)R_1(18)+ wag(C–H)R_2(15)
55	699	677	–	–	1.94	4.97	β(C–C–O)Pr(39) + wag (C–H)R_1(25)
56	637	617	624	618	4.06	4.60	β(C–C–C)R_2(66)
57	620	600	603	603	1.19	1.73	β_{out}(C–C–C)Pr(30)+β_{out}(C–C–C)R_1(27) + β_{out} (O–C–C) Pr(24)
58	608	588	–	582	35.21	4.36	β(C–C–C)R_2(40) + β(C11–C8–C3)(35)
59	540	522	534	542	0.4694	18.79	β(C–C–C)Pr(57)+β(C–C–C) R_1(23)
60	536	519	520	509	0.46	2.32	β(C–C–C)Pr(39)+β(C–C–C) R_1 (25)
61	505	489	492	495	13.82	2.08	Ring R_2 Torsion(41)+Pr Ring torsion(26) +Ring R_1 Torsion(23)
62	496	480	462	–	8.29	2.47	Ring R_2 Torsion (43)+ Ring R_1 torsion(29) +ρ(C4–C3–C8–C11)(26)
63	444	430	–	432	0.19	0.64	Ring R_1 torsion(54)+ ρ(O–C–C–C)Pr(24) +ρ(C–C–C–C)Pr(17)
64	413	400	–	400	0.01	0.07	Ring R_2 Torsion(91)

Note: Abbreviations have following meanings - ν-streching, ν_s-symmetric stretching, ν_{as}-asymmetric stretching , β-bending , β_{out}-out of plane bending, čl-torsion

*FTIR and Raman experimental data taken `www.sigmaaldrich.com/united-states.html` website.

4.3.1 Phenyl ring vibrations

The phenyl ring spectral region predominantly involves the C–H, C–C and C–C stretching, and C–C–C as well as H–C–C–bending vibrations. There are two benzene rings R_1 and R_2, where R_1 is a part of indadione ring and R_2 is attached to the flap carbon atom. The bands due to the ring C–H-stretching vibrations were observed as a group of partially overlapping absorptions in the region 3100–3000 cm^{-1}. The calculated wavenumber for the CH-stretching modes are found in the range 3096–3055 cm^{-1} and have been matched with the experimental FTIR and FT Raman spectra. Vibrations involving C-H in-plane bending are found throughout the region 1600–997 cm^{-1}. The computed bands at 1478 and 985 cm^{-1} are due to semicircle stretching and trigonal ring bending of the R_2, and are matched well with experimentally observed bands at 1480/1470 cm^{-1} and 979/987 cm^{-1} in FTIR and FT Raman spectra. The dominant H–C–C in-plane bending of the R_1 ring with more than 70% contribution to the total PED was calculated to be 1145 and 1143 cm^{-1} and correspond to the peaks at 1146 and 1150 cm^{-1} in the Raman and FTIR spectra. The C–H wagging mode starts appearing from 985 cm^{-1} and has contributions up to 677 cm^{-1} and are assigned well in both the spectra. The torsional modes appear in general in the low-wavenumber regions. In the present case, the calculated normal modes below 500 cm^{-1} wavenumbers are mainly the torsional modes.

4.3.2 C=O group vibrations

The appearance of strong bands in the FT-IR and weak bands in the Raman spectra (less polarizability resulting due to highly dipolar carbonyl bond) around 1650–1800 cm^{-1} in aromatic compounds shows the presence of carbonyl group and is due to the C=O-stretching motion. The wavenumber of the stretch due to carbonyl group mainly depends on the bond strength which in turn depends upon inductive, conjugative, field and steric effects. The calculated wavenumber at 1752 and 1719 cm^{-1} (with PE.D. contribution of 88% and 90%) corresponding to symmetric and asymmetric C=O stretching vibrations, are assigned with the bands at 1747, 1714 cm^{-1}/ 1748 and 1710 cm^{-1} respectively in FTIR/ FT Raman spectra. These calculated bands appear as coupled modes and have been assigned well with the corresponding experimentally observed peaks. The corresponding peaks in the Raman spectra are found to be weak due to the less polarizable C=O bond. The small discrepancy between the calculated and the observed wavenumbers may be due to the intermolecular hydrogen bonding [1]. The bands calculated at 852 and 786 cm^{-1} are identified as C=O out-of-plane bending modes while the normal modes calculated at 679 and 677 cm^{-1} are identified as in plane C=O bending vibrations.

5 Conclusion

The equilibrium geometry and harmonic frequencies of phenindione under investigation were determined and analyzed at DFT level employing the 6-311++G(d,p) basis set. The skeleton of the optimized molecule is found to be non-planar. In general, a good agreement between experimental and calculated normal modes of vibrations have been observed. According to

the frontier orbital energy gap and the dipole moment data, the phenindione is slightly more reactive molecule and more polarizable, than its ancestor molecule. The molecular electrostatic potential surface study has also been employed successfully to explain the property of 2-pheny-1H-indene- 1,3(2H)-dione over its ancestor. The present quantum chemical study may further play an important role in understanding of dynamics of the molecule.

References

[1] D. J. Naisbitt, J. Farrell, and P. J. Chamberlain, J. Pharmacol. Exp. Ther. 313 (2005) 1058.
[2] M. Walis and R. Autor, Nursing Standard 15 (2001) 47.
[3] J. D. Pipkin and V. J. Stella, J. Am. Chem. Soc. 104 (1982) 6672.
[4] http://www.sigmaaldrich.com/united-states.html.
[5] A. D. Becke, J. Chem. Phys. 98 (1993) 5648.
[6] C. Lee, W. Yang, and R. G. Parr, Phys. Rev. B 37 (1988) 785.
[7] B. Miehlich, A. Savin, H. Stoll, and H. Preuss, Chem. Phys. Lett. 157 (1989) 200.
[8] W. Kohn and L. J. Sham, Phys. Rev. 140 (1965) A1133.
[9] M. J. Frisch, G. W. Trucks, H. B. Schlegel, *et al.*, Gaussian 09, Rev. A.1 (Gaussian, Inc., Wallingford CT, 2009).
[10] A. P. Scott and L. Random, J. Phys. Chem. 100 (1996) 16502.
[11] P. Pulay, G. Fogarasi, G. Pongor, *et al.*, J. Am. Chem. Soc. 105 (1983) 7037.
[12] A. Frisch, H. P. Hratchian, R. D. Dennington II, *et al.*, Gaussview, Ver. 5.0 (Gaussian, Inc., Wallingford CT, 2009).
[13] M. H. Jamroz, Vibrational Energy Distribution Analysis: VEDA 4 Program (Warsaw, Poland, 2004).
[14] G. Keresztury, S. Holly, J. Varga, *et al.*, Spectrochim. Acta A 49 (1993) 2007.
[15] G. Keresztury, in Raman Spectroscopy: Theory- Handbook of Vibrational Spectroscopy, eds. J. M. Chalmers and P. R. Griffith (John Wiley & Sons, New York, 2002).
[16] C. Knox, V. Law, T. Jewison, *et al.*, Nucleic Acids Res. 39 (2011) D1035; D. S. Wishart, C. Knox, *et al.*, M. 16 Hassanali. Nucleic Acids Res. 36 (2008) D901; D. S. Wishart, C. Knox, A. C. Guo, *et al.*, Nucleic Acids Res. 34 (2006) D668.
[17] L. A. Chetkina and V. K. Belsky, Crystallogr. Rep. 53 (2008) 618.
[18] M. Ladd, Introduction to Physical Chemistry, third ed. (Cambridge University Press, Cambridge, 1998).
[19] I. Fleming, Frontier Orbitals and Organic Chemical Reactions (John Wiley & Sons, New York, 1976).
[20] J. S. Murray and K. Sen, Molecular Electrostatic Potentials, Concepts and Applications (Elsevier, Amsterdam, 1996).
[21] I. Alkorta and J. J. Perez, Int. J. Quant. Chem. 57 (1996) 123.
[22] E. Scrocco and J. Tomasi, in: Advances in Quantum Chemistry, ed. P. Lowdin (Academic Press, New York, 1978).
[23] F. J. Luque, M. Orozco, P. K. Bhadane, and S. R. Gadre, J. Phys. Chem. 97 (1993) 9380.

[24] J. Sponer and P. Hobza, Int. J. Quant. Chem. 57 (1996) 959.
[25] R. K. Pathak and S. R. Gadre, J. Chem. Phys. 93 (1990) 1770.
[26] S. R. Gadre and I. H. Shrivastava, J. Chem. Phys. 94 (1991) 4384.